Polymer Chemistry

Ambient-Dried Highly Flexible Copolymer Aerogels and their Nanocomposites with Polypyrrole for Thermal Insulation, Separation, and Pressure Sensing

Journal:	*Polymer Chemistry*
Manuscript ID	PY-ART-05-2019-000751.R1
Article Type:	Paper
Date Submitted by the Author:	21-Jul-2019
Complete List of Authors:	Zu, Guoqing; Tongji University, School of Materials Science and Engineering Kanamori, Kazuyoshi; Kyoto University Maeno, Ayaka; Kyoto University Kaji, Hironori; Kyoto University Nakanishi, Kazuki; Kyoto University Shen, Jun; Tongji University

ARTICLE

Ambient-Dried Highly Flexible Copolymer Aerogels and their Nanocomposites with Polypyrrole for Thermal Insulation, Separation, and Pressure Sensing

Received 00th January 20xx,
Accepted 00th January 20xx

DOI: 10.1039/x0xx00000x

Guoqing Zu,* [a] Kazuyoshi Kanamori,* [b] Ayaka Maeno, [c] Hironori Kaji, [c] Kazuki Nakanishi, [b] and Jun Shen [d]

Aerogels possess unique properties but their practical applications have been restricted by low mechanical strength and costly supercritical drying; it remains difficult to obtain highly flexible aerogels with good thermal insulation and absorption by ambient pressure drying (APD). Here we report novel highly flexible aerogels based on polyvinylpolymethylsiloxane (PVPMS)/polyvinyltrimethylsilane (PVTMS) co-network, which consists of inter-crosslinked hydrocarbon and siloxane polymers with dangling trimethylsilyl groups, and its nanocomposite with polypyrrole (PPy). The PVPMS/PVTMS copolymer aerogels are facilely synthesized by a consecutive radical co-polymerization and hydrolytic polycondensation strategy from two monomers vinylmethyldimethoxysilane and trimethylvinylsilane without additional crosslinkers, followed by APD without any post-gelation modification. The PPy nanocomposite aerogels are synthesized by an in-situ oxidation polymerization of pyrrole in the copolymer aerogel networks, followed by APD. The resulting aerogels consist of meso- to macro-scaled pore structures with tunable skeleton and pore sizes with variable crosslinking density and bulk density. In addition, these aerogels show good hydrophobicity and high flexibility in both compression and bending. Moreover, different functionalities such as excellent thermal insulation, oil-water separation, and pressure sensing can be imparted, allowing them to exhibit potential applications in thermal insulation, separation, and sensing.

Introduction

Aerogels are highly porous materials with a variety of unique properties such as low bulk density, high porosity, high specific surface area (SSA), and low thermal conductivity.[1-3] Because of their unique properties, aerogels are recognized as suitable candidates for a wide range of applications including adsorption/absorption,[4,5] thermal insulation,[6-8] catalysis, [9,10] energy storage,[11,12] smart sensing,[13] and cosmic dust collection.[14] The widely studied silica aerogels and other inorganic aerogels are, however, usually brittle (friable) because of their three-dimensional solid skeletons composed of weakly connected nanoparticles, and the low mechanical strength badly restricts their practical applications.

In order to improve the mechanical strength, many efforts have been made to prepare flexible aerogels with compressibility or bendability by a variety of methods. Crosslinking of inorganic aerogels with organic polymers such as polyimide, epoxy, polystyrene, polyurea, and polynorbornene, gave compressible or bendable aerogels, but usually sacrificed porosity and thermal insulation ability, because the pores were partially filled and blocked by the polymers.[15-17] Interpenetrating inorganic and organic networks (not inter-connected) was also used to reinforce aerogels.[2,18] Crosslinking of organic polymers via a specific method may lead to flexible aerogels. The reported organic aerogels based on polyimide, [19] poly(vinyl alcohol),[5] resorcinol-formaldehyde,[20] polythiophene-based thermoelectric polymers[21] showed good compressibility or elasticity. Crosslinking or physical assembly of fibers such as nanocellulose,[8] chitosan,[22] natural wood fibers,[23] konjac glucomannan,[13] and silica nanofibers[24] also afforded aerogels with compressibility or bendability. Another method to prepare compressible and elastic aerogels was crosslinking or physical assembly of graphenes or carbon nanotubes.[25,26] Polyorganosiloxane-based hybrid networks obtained through hydrolysis and polycondensation of trifunctional organoalkoxysilanes[27,28] and organo-bridged alkoxysilanes[4,29] were found to be successful in drastically improving compressibility and elasticity. Nonetheless, bending flexibility of the aerogels obtained via these methods was still not satisfactory for practical applications.

Besides, in the preparation of aerogels, special drying techniques such as supercritical drying (SD) under high pressure/temperature were usually used to replace the pore liquid with air to maintain the fragile/brittle network.[2] The costly drying process also significantly limited their practical applications. Several drying techniques other than SD such as vacuum drying (VD)[4] and freeze drying (FD)[25,30,31] have been applied to prepare aerogels. However, these drying processes involved low pressure or low temperature, which made

[a] School of Materials Science and Engineering, Tongji University, Shanghai 201804, P. R. China. E-mail: guoqingzu@tongji.edu.cn.
[b] Department of Chemistry, Graduate School of Science, Kyoto University, Kitashirakawa, Sakyo-ku, Kyoto 606-8502, Japan. E-mail: kanamori@kuchem.kyoto-u.ac.jp
[c] Institute for Chemical Research, Kyoto University Gokasho, Uji, Kyoto 611-0011, Japan
[d] Shanghai Key Laboratory of Special Artificial Microstructure Materials and Technology, Pohl Institute of Solid State Physics, Tongji University, Shanghai 200092, P. R. China.
Electronic Supplementary Information (ESI) available: GPC data, Uniaxial compression–decompression, three-point bending, and hand bending tests, recycle performance (PDF); Compression and bending flexibility, separation, strain-sensitive conductivity (AVI). See DOI: 10.1039/x0xx00000x

them energy-consuming, also limiting practical applications. In addition, these drying techniques including SD suffered from limitation in scaling up. A promising alternative drying technique to prepare aerogels was ambient pressure drying (APD).[32-33] The APD process was more compatible with scaling up; however, traditional APD usually needed additional surface modification and the obtained aerogels via APD usually exhibit serious cracking.[34,35] It remains difficult to obtain highly bendable aerogels with excellent thermal insulation and absorption by APD.

Recently, we have obtained flexible aerogels based on polyvinylpolymethylsiloxane (PVPMS), polyallypolymethylsiloxane (PAPMS), and polyallypolysilsesquioxane (PAPSQ).[36,37] The obtained aerogels showed a unique double crosslinked structure and combined transparency, good flexibility and thermal insulation. In order to further enhance the mechanical properties, aerogels based on polyvinylpolydimethylsiloxane (PVPDMS) have been prepared.[38] The PVPDMS aerogels exhibited higher bending flexibility and excellent absorption capacity for organic solvents and oils. Flexible composite aerogels based on PVPDMS/graphene with a strain sensing performance have also been prepared via this method. However, the reported PVPDMS aerogels and PVPDMS/graphene composite aerogels were obtained via FD instead of APD.

Here, we report a new type of aerogels based on the PVPMS/PVTMS copolymer network and its nanocomposite with polypyrrole (PPy) with improved flexibility via simple APD. The copolymer aerogels were synthesized by a facile strategy that involves consecutive radical co-polymerization and hydrolytic polycondensation without additional crosslinkers. Two precursors vinylmethyldimethoxysilane (VMDMS, CH_2=CHSi(CH_3)(OCH_3)$_2$) and trimethylvinylsilane (TMVS, CH_2=CHSi(CH_3)$_3$) were first radically co-polymerized to give linear polyvinylmethyldimethoxysilane (PVMDMS)/polyvinyltrimethylsilane (PVTMS) copolymer. The obtained copolymers were then subjected to hydrolytic polycondensation followed by APD without any modification to afford PVPMS/PVTMS copolymer aerogels consisting of polymethylsiloxanes (PMS) and hydrocarbon polymers that were crosslinked with each other. The PVPMS/PVTMS/PPy nanocomposite aerogels consisting of PMS, hydrocarbon polymers, and PPy were synthesized by an *in-situ* oxidation polymerization of pyrrole in the copolymer aerogels, followed by the same APD technique. The resulting aerogels exhibited tunable porous structures, hydrophobicity, and high compressibility and bendability with elasticity. In addition, they combined excellent thermal insulation, oil–water separation, and pressure sensing.

The incorporation of TMVS led to PVPMS/PVTMS copolymer aerogels with significantly enhanced bending flexibility compared to that of pristine PVPMS aerogels. Their bending flexibility was also much higher than that of PAPMS and PAPSQ aerogels. In addition, the PVPMS/PVTMS/PPy nanocomposite aerogel was conductive because PPy was well distributed in the network of the composite aerogel, and exhibited a better compression cycle performance compared to that of the conductive PVPDMS/graphene composite aerogel. These aerogels obtained via this simple APD showed significant advantages in practical applications of thermal insulation, separation, and pressure sensing over conventional aerogels and the reported PVPDMS and PVPDMS/graphene aerogels obtained via FD. The relationship of the synthesis parameters, structures, mechanical properties, and the resulting functionalities are discussed.

Results and disscussion

Synthesis

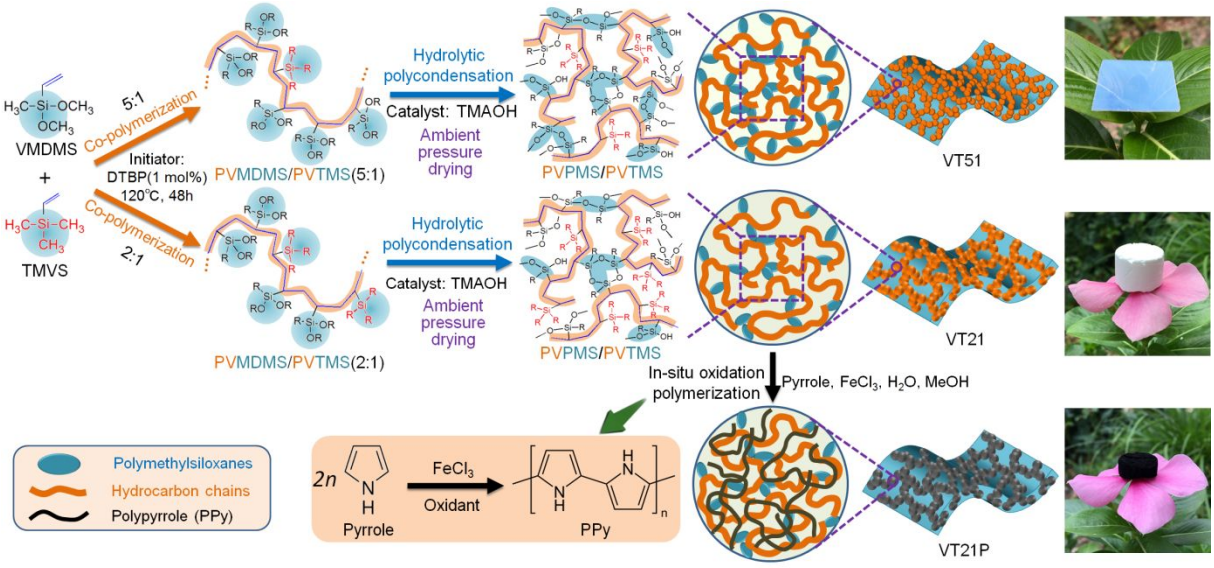

Fig. 1 Synthesis of PVPMS/PVTMS copolymer aerogels via a facile strategy that involves consecutive radical co-polymerization and hydrolytic polycondensation. PVPMS/PVTMS/PPy nanocomposite aerogels are also prepared by combining with *in-situ* oxidation polymerization of pyrrole. The molar ratio of VMDMS to TMVS is 5:1 for VT51, while that is 2:1 for VT21.

Fig. 1 schematically presented the synthesis procedures of PVPMS/PVTMS-based copolymer aerogels. Di-*tert*-butyl peroxide (DTBP) was used as the radical initiator in radical co-polymerization. The polymerization time, temperature, and DTBP concentration

were fixed at 48 h, 120 °C, and 1 mol %, respectively. The results on the co-polymerization of VMDMS and TMVS with the molar ratios of 5:1 and 2:1 are listed in Table 1. The weight-average molecular weight (M_w), obtained by gel permeation chromatography (GPC) (Fig. S1), of PVMDMS/PVTMS copolymers with the molar ratio of 5:1 and 2:1 was 4995 and 4149, respectively, indicating high degrees of polymerization. The polydispersity (M_w/M_n) of the copolymers was in the range of 1.77−1.80. Monolithic copolymer gels formed after hydrolysis and polycondensation in the presence of a strong base catalyst tetramethylammonium hydroxide (TMAOH). In addition, iron (III) chloride was used as the initiator to promote *in-situ* oxidation polymerization of pyrrole in PVPMS/PVTMS copolymer aerogels to afford PVPMS/PVTMS/PPy nanocomposite aerogels.

Table 1. Results on the co-polymerization of VMDMS and TMVS with the molar ratios of 5:1 and 2:1.

Precursor	VMDMS/TMVS /mol mol^{-1}	DTBP /mol%	Polymerization time /h	M_w	M_w/M_n
VMDMS/TMVS	5:1	1	48	4995	1.80
VMDMS/TMVS	2:1	1	48	4149	1.77

Tunable microstructure

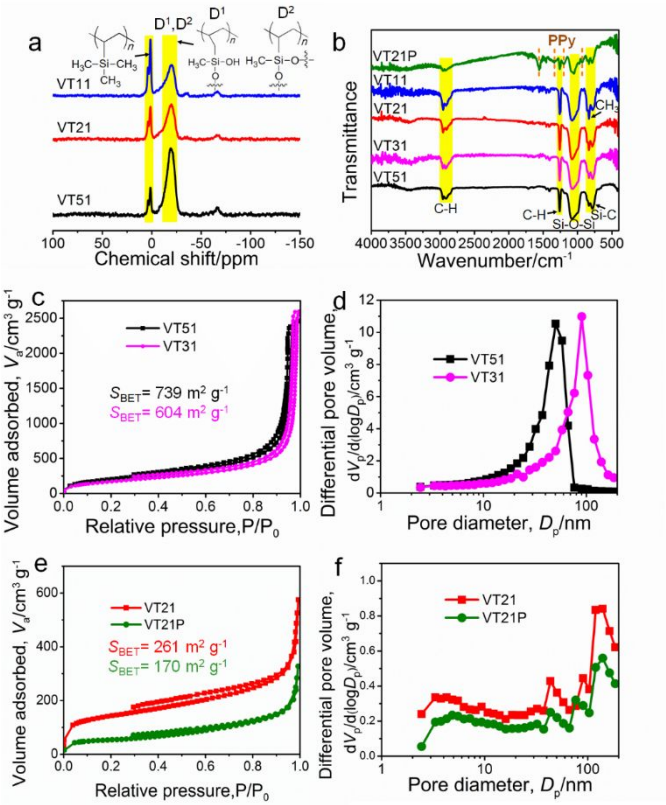

Fig. 2 (a) ^{29}Si CP/MAS NMR spectra of typical aerogels. b) FTIR spectra of typical copolymer and nanocomposite aerogels. (c) N_2 adsorption/desorption isotherms and (d) BJH pore size distributions of VT51 and VT31. (e) N_2 adsorption/desorption isotherms and (f) BJH pore size distributions of VT21 and VT21P.

The chemical structure of PVPMS/PVTMS copolymer aerogels was investigated by the ^{29}Si CP/MAS NMR spectra as shown in Fig. 2a. The peak around −20 ppm corresponded to D^2 $(CH_2CH(Si(CH_3)O_{2/2}))_n$ and D^1 species, while that around 1.4 ppm corresponded to $(CH_2CH(Si(CH_3)_3))_n$ species. [39] These peaks indicated the co-presence of two inter-crosslinked networks, namely PMS and hydrocarbon polymers, in the PVPMS/PVTMS copolymer aerogels. Besides, it was found that the intensity of the peak around −20 ppm decreased while that of the peak around 1.4 ppm increased with increasing the molar ratio of TMVS to VMDMS in the precursors. This indicated that there were less PMS and more trimethylsilyl groups in the PVPMS/PVTMS copolymer aerogels with increasing the molar ratio of TMVS to VMDMS. In our previous work, the peak corresponding to the silicon with vinyl groups (CH_2=$CH(CH_3)SiO_{2/2}$) were detected at around −35 ppm in NMR spectra.[36] This peak was negligible for VT51, VT21, and VT11 (Fig. 2a), indicating that almost all monomer molecules containing vinyl groups reacted during polymerization.

The molecular structure of aerogels based on PVPMS/PVTMS (VT51, VT31, VT21, and VT11) and PVPMS/PVTMS/PPy (VT21P) copolymers were also investigated by the FTIR spectra as shown in Fig. 2b. The bands located at 2953 cm^{-1} and 2908 cm^{-1} were attributed to the stretching of C−H bonds while that at 1260 cm^{-1} was to the asymmetric deformation of C−H bonds.[36] These C−H bonds were supposed to result from the hydrocarbon chains and $-CH_3$ groups in the PVPMS/PVTMS aerogels. The absorption bands at ~1070 cm^{-1}, 830 cm^{-1}, and 780 cm^{-1} were ascribed to the stretching of Si−O−Si bonds, rocking of CH_3, and asymmetric stretching of Si−C bonds, respectively. [37,40] These bands indicated the methyl-rich PMS and trimethylsilyl groups in PVPMS/PVTMS aerogels. The abundant CH_3 groups and hydrocarbon chains and a low concentration of –OH groups rendered these aerogels hydrophobic with the water contact angle (WCA) of >130°. Aerogels VT21 and VT11 exhibited high hydrophobicity with WCA as high as ~158°, which was higher than those of VT51 (136°) and VT31 (145°) (the insets of Fig. 3). The higher WCA was probably attributed to the larger amount of $-CH_3$ groups in VT21 and VT11 and coarsened pore structure as discussed later.

In the case of VT21P, the FTIR spectrum showed not only the bands mentioned above but also new bands at 1560 cm^{-1}, 1327 cm^{-1}, 1200 cm^{-1}, and 925 cm^{-1} corresponding to C−C, C−H, C−N, and C−H bonds, respectively, which resulted from PPy in the aerogel.[41,42] This confirmed that PVPMS/PVTMS/PPy nanocomposite aerogel VT21P exhibited a composite structure consisting of PMS, hydrocarbon chains, and PPy. Because of the abundance of CH_3 groups and hydrocarbon chains, VT21P showed hydrophobicity similar to VT21. The FTIR spectrum measured from the center and surface of the sample VT21P was the same, indicating that PPy was well distributed in the network of the composite aerogel.

A crucial step for the synthesis of aerogels was the drying process. In the case of APD, wet gels usually underwent large temporal volume shrinkage due to the capillary force exerted on the entire thin gel skeletons during evaporation of the solvent in the wet gels upon APD. If there was a large number of –OH groups on the surface of the

gel skeletons, condensation of adjacent –OH groups occurred during APD, which would result in irreversible shrinkage of the gels. The gels without compressibility or elasticity would also suffer irreversible shrinkage or cracking during APD. In this case, it was difficult to obtain monolithic aerogels with low bulk density via APD.

One of the advantages of these copolymer aerogels over conventional aerogels is that these aerogels can be prepared via APD without any surface modifications such as hydrophobization with silylating agents. The obtained PVPMS/PVTMS copolymer aerogels possessed a copolymer network structure with a low concentration of –OH groups and abundant inert hydrophobic CH_3 groups. The copolymer network structure exhibited high compressibility and elasticity, which was confirmed below. Benefiting from their unique structure, the PVPMS/PVTMS copolymer wet gels underwent large temporal volume shrinkage without fracture upon APD and then sprang back to nearly their original sizes after the solvent in the gels was completely evaporated, successfully affording monolithic PVPMS/PVTMS copolymer aerogels with low bulk density.

It was difficult to obtain aerogels with bulk density lower than 80 mg cm^{-3} via APD without modifications in the systems of PVPMS, PAPMS, and PVPDMS. However, monolithic PVPMS/PVTMS copolymer aerogels (VT51, VT31, VT21, VT21P, and VT11) with low density in the wide range of 40–210 mg cm^{-3} were easily obtained via APD without any modifications. Since this APD process requires no surface modifiers, the aerogels obtained via this method are promising for practical applications.

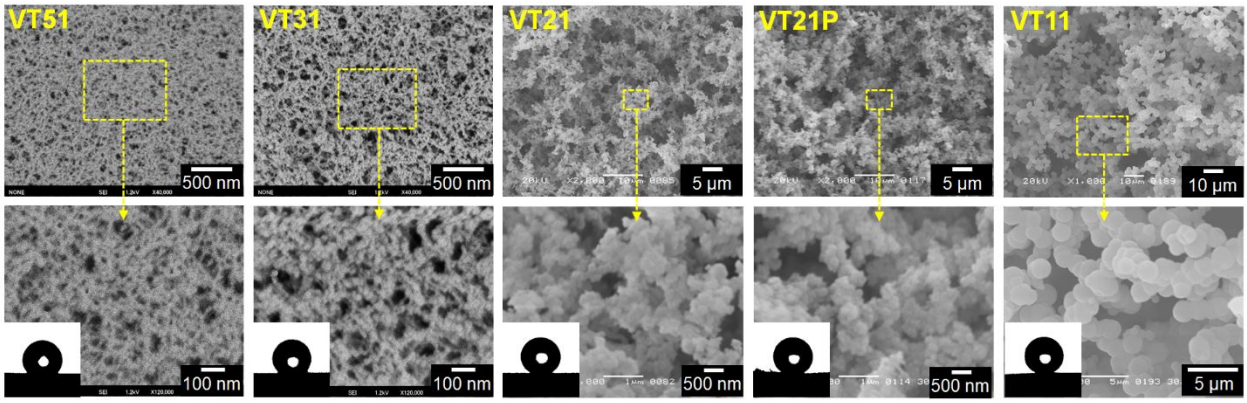

Fig. 3 SEM images of typical aerogels. The insets present WCA on each aerogel. The obtained aerogels exhibit tunable sizes of particulate skeletons and pores and tunable hydrophobicity.

The highly porous structure was confirmed by N_2 adsorption/desorption measurements and SEM images (Fig. 2c-f and Fig. 3). The molar ratio of VMDMS to TMVS significantly affected the porous structure of the resulting aerogels. With the relatively high molar ratio of VMDMS to TMVS (5:1), the aerogels contained abundant PMS with lower hydrophobicity and a small amount of trimethylsilyls with higher hydrophobicity, which resulted in the networks with relatively lower hydrophobicity and higher crosslinking density. In this case, macroscopic phase separation during hydrolytic polycondensation was suppressed, leading to a homogenous structure with small nano-sized particulate skeletons and pores (Fig. 3), affording translucent aerogels (VT51) with visible-light transmittance of 69 % at wavelength of 550 nm for the sample of 1 mm thickness.[28]

Table 2. Starting compositions and physical properties of typical aerogels.

sample	VMDMS /mL	VMDMS /TMVS /mol mol^{-1}	DTBP /mol%	BzOH /VMDMS /mol mol^{-1}	H_2O /VMDMS /mol mol^{-1}	TMAOH /VMDMS /mol mol^{-1}	ρ[a] /mg cm^{-3}	S_{BET}[b] /m^2 g^{-1}	d[c] /nm
VT51	1	5:1	1	5.1	2	0.052	210	739	50
VT31	1	3:1	1	5.5	2	0.052	205	604	90
VT21	1	2:1	1	26.7	16	0.167	44	261	140
VT11	1	1:1	1	31.8	13	0.209	43	-	-
VT21P	1	2:1	1	26.7	16	0.167	73	170	140

[a] Bulk density. [b] SSA obtained from nitrogen adsorption measurement using Brunauer-Emmett-Teller (BET) calculation. [c] Mean pore diameter obtained from nitrogen adsorption branch via the Barrett-Joyner-Halenda (BJH) method.

With a lower molar ratio of VMDMS to TMVS (3:1, 2:1, and 1:1), however, the aerogels exhibited networks with higher hydrophobicity and lower crosslinking density. In this case, the macroscopic phase separation proceeded, resulting in an inhomogeneous structure with larger particulate skeletons and pores (Fig. 3). Accordingly, the SSA decreased and sizes of skeletons and pores increased with decreasing the molar ratio of VMDMS to TMVS (Table 2 and Fig. 3). The SSA decreased from 739 m^2 g^{-1} for VT51 to 604 m^2 g^{-1} for VT31 and then 261m^2 g^{-1} for VT21. The sample VT51 exhibited a narrow pore size distribution mainly in the range of 10–80 nm, while VT31 showed a wider pore size distribution mainly in the range of 20–150 nm. The sample VT21 had much less pores in the range of 10–200 nm compared to those of VT51 and VT31. The samples VT51 and VT31 exhibited relatively small particle sizes of

20−70 and 30−100 nm, respectively, whereas VT21 and VT11 showed relatively large particle sizes of 100−400 nm and 1−2.5 μm, respectively. These results indicated that the porous structure of the resulting aerogels was highly tunable, which was achieved simply by adjusting the ratio of TMVS in the precursors. The bulk density was also tunable (40−210 mg cm^{-3}) simply by adjusting the concentration of the precursors during preparation (Table 2). In addition, the macropores were well preserved after the incorporation of PPy in the copolymer aerogels (Figure 3, VT21P). However, the mesopore volume and SSA decreased after the incorporation of PPy because PPy blocked considerable mesopores and small macropores and lowered the porosity (Fig. 2e,f). The WCA on these aerogels became higher with increasing TMVS, since the roughness of the surface became higher and the network became intrinsically more hydrophobic (less surface energy) as discussed earlier. Also, the air pockets inside the pores would produce 'lotus leaf' effects, preventing wetting.

In spite of the highly porous structure consisting of relatively small particles, the copolymer and nanocomposite aerogels exhibited high compressibility and elasticity as shown in Fig. 4a-d. In the case of VT51, VT31, and VT21, they were compressed with maximum 80 % strain without fracture and then sprang back to their original size rapidly (in two seconds) after the force was removed in the uniaxial compression-decompression tests. In the case of VT21P and VT11, they also showed spring-back from 50 % compression without fracture (Fig. 4c, Fig. S2 and S3). The movie of a hand compression test clearly presented the high compressibility and elasticity of VT21P (Movie S1). In addition, VT21 and VT21P also underwent spring-back to nearly their original sizes after 200 cycles of uniaxial compression-decompression with maximum 50 % strain (Fig. 4b,c). Their morphology remained nearly unchanged after 100 cycles as presented in Fig. S4 and Fig. S5, indicating an excellent compression cycle performance. The compression cycle performance of the PVPMS/PVTMS/PPy nanocomposite aerogel (VT21P) was better than that of the reported PVPDMS/graphene composite aerogel.[38]

Mechanical flexibility

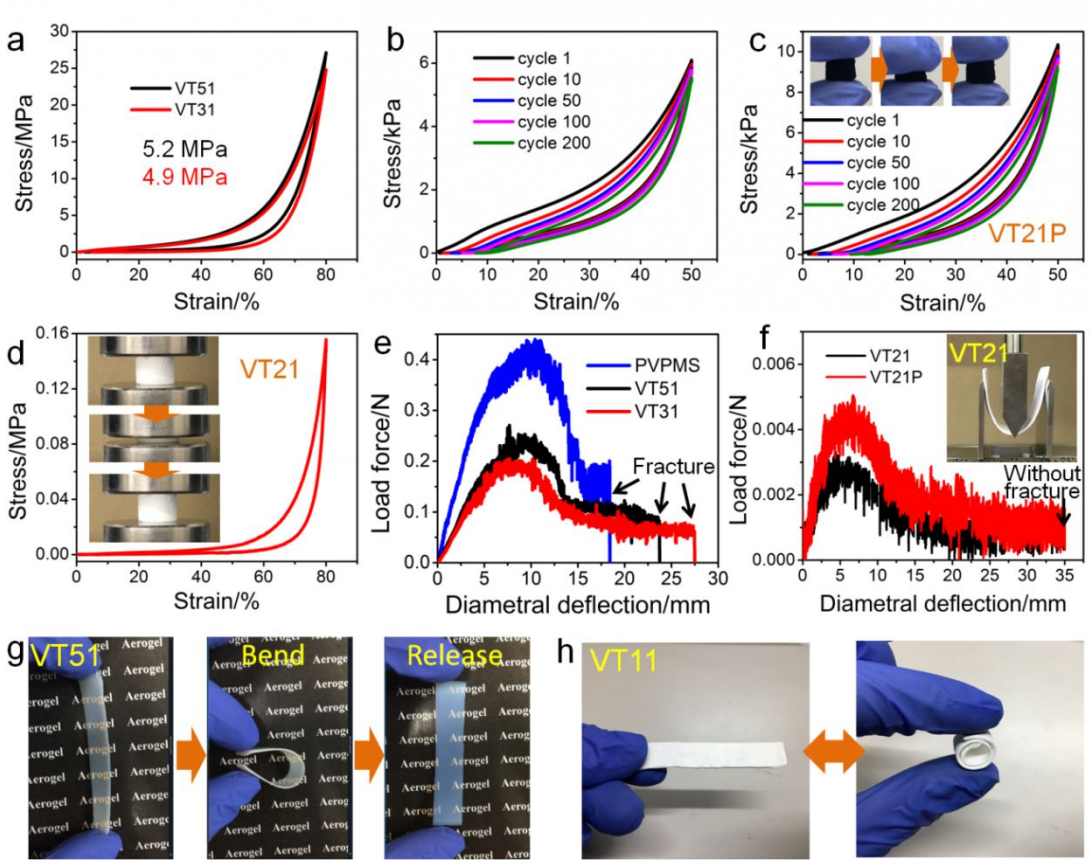

Fig. 4 (a-d) Stress-strain curves of uniaxial compression−decompression tests on typical aerogels. The values in (a) are the obtained Young's moduli. The insets of (c) are the photographs of a hand compression test on VT21P. The insets of (d) are the photographs of a uniaxial compression−decompression test on VT21. (e,f) Stress−strain curves of three-point bending tests on typical aerogels. The stress-strain curve marked with PVPMS in (e) is obtained from pristine PVPMS aerogel (AH1-48-1-100) *via* APD for comparison.[36] The inset of (f) is a three-point bending test on VT21. (g,h) Hand bending tests on typical aerogels, showing high bending flexibility.

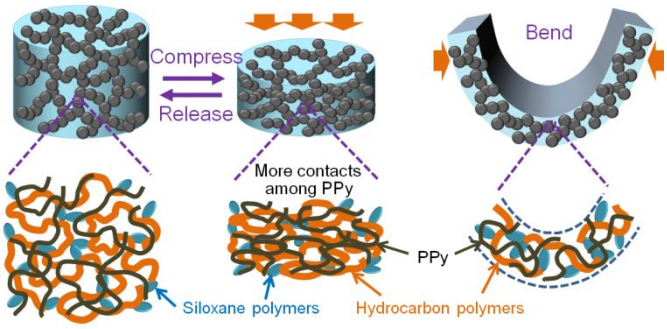

Fig. 5 Schematic of microstructure variations during compression and bending tests for PVPMS/PVTMS/PPy nanocomposite aerogels.

In addition, these aerogels exhibited high flexibility in bending as shown in Fig. 4e-h, Fig. S6, and Fig. S7. They underwent a large diametral deflection of 22−35 mm without fracture and then showed spring-back to nearly their original shapes in the three-point bending tests with a fixture span of 25 mm and specimen size of 10 × (60−70) × 1 mm. With increasing diametral deflection during three-point bending tests, the whole sample would move down, resulting in the force of friction between samples and two fixtures, which led to large oscillations of the stress−strain curves. The large oscillations before fracture did not indicate the structural damage in the materials. They could also be bent by hand with a large angle without fracture and then showed nearly perfect spring-back after they were released. The movie of a hand bending test clearly demonstrated the high bending flexibility of VT51 (Movie S2). In addition, the bendability was effectively enhanced by increasing TMVS (Fig. 4e,f,h). As shown in Fig. 4h, sample VT11 can even be rolled up without fracture. The high flexibility of the PVPMS/PVTMS copolymer aerogels and their nanocomposites with PPy was attributed to their unique copolymer networks consisting of flexible hydrocarbon polymers and PMS. Fig. 5 schematically presented the microstructure variations during compression and bending for PVPMS/PVTMS/PPy nanocomposite aerogels.

The bending flexibility of these ambient-dried PVPMS/PVTMS copolymer aerogels was apparently higher than that of PVPMS, PAPMS, PAPSQ, and polymethylsilsesquioxane (PMSQ) aerogels with similar bulk density. [36,37] By comparing the stress−strain curves of three-point bending tests on PVPMS/PVTMS aerogel with the molar ratio of VMDMS to TMVS of 2:1 (VT21, Fig. 4f) and reported PVPDMS/PVPMS aerogel with the molar ratio of VMDMS to vinyldimethylmethoxysilane (VDMMS) of 2:1 (PA4), [38] PVPMS/PVTMS aerogels showed higher bending flexibility compared to that of PVPDMS/PVPMS aerogels with the same molar ratio of VMDMS to the co-precursor (TMVS or VDMMS). TMVS molecule had more inert hydrophobic groups and less reactive groups (with three methyl groups and one reactive vinyl group) compared to those of VDMMS (with two methyl groups and two reactive groups—one vinyl group and one methoxy group). Therefore, as the co-precursor of VMDMS for the copolymer aerogels, TMVS was supposed to be more effective for lowering crosslinking density and enhancing hydrophobicity compared to those of VDMMS. The lower crosslinking density may lead to higher deformability, contributing to the higher bending flexibility.

Thermal insulation, separation, and pressure sensing

Because of their unique copolymer structure, the resulting aerogels exhibited several outstanding properties as shown below. Since they possessed relatively low bulk density (200−210 mg cm^{-3}) and a highly porous interconnected three-dimensional network structure that was composed of small nanoparticles (20−100 nm) and nanopores (10−150 nm), the solid and gas thermal conductions of VT51 and VT31 were suppressed. As a result, the copolymer aerogels VT51 and VT31 exhibited low thermal conductivities of 15.8 and 16.6 mW m^{-1} K^{-1} (Fig. 6a), respectively at room temperature and ambient pressure. Because VT51 showed relatively smaller particles and pores compared to those of VT31, the solid and gas thermal conductions of VT51 were more effectively suppressed, leading to the lower thermal conductivity of VT51 compared to that of VT31. The thermal conductivities of VT51 and VT31 were much lower than those of stationary air (ca. 26 mW m^{-1} K^{-1})[8] and commercial thermal insulators such as mineral wool (35−80 mW m^{-1} K^{-1})[14] and comparable to those of conventional silica aerogels (14−25 mW m^{-1} K^{-1}), [35,43] pristine PVPMS aerogels (15−16 mW m^{-1} K^{-1}), [36] PMSQ aerogels (15−35 mW m^{-1} K^{-1}), [44] and polyvinylsilsesquioxane (PVSQ) aerogels (15.3 mW m^{-1} K^{-1}),[27] indicating an excellent thermal insulation performance. In addition, the thermal conductivity of VT31 was comparable to those of PVPDMS/PVPMS composite aerogels (16.2−17.6 mW m^{-1} K^{-1}), while the thermal conductivity of VT51 was slightly lower than those of PVPDMS/PVPMS composite aerogels. [38]

ARTICLE

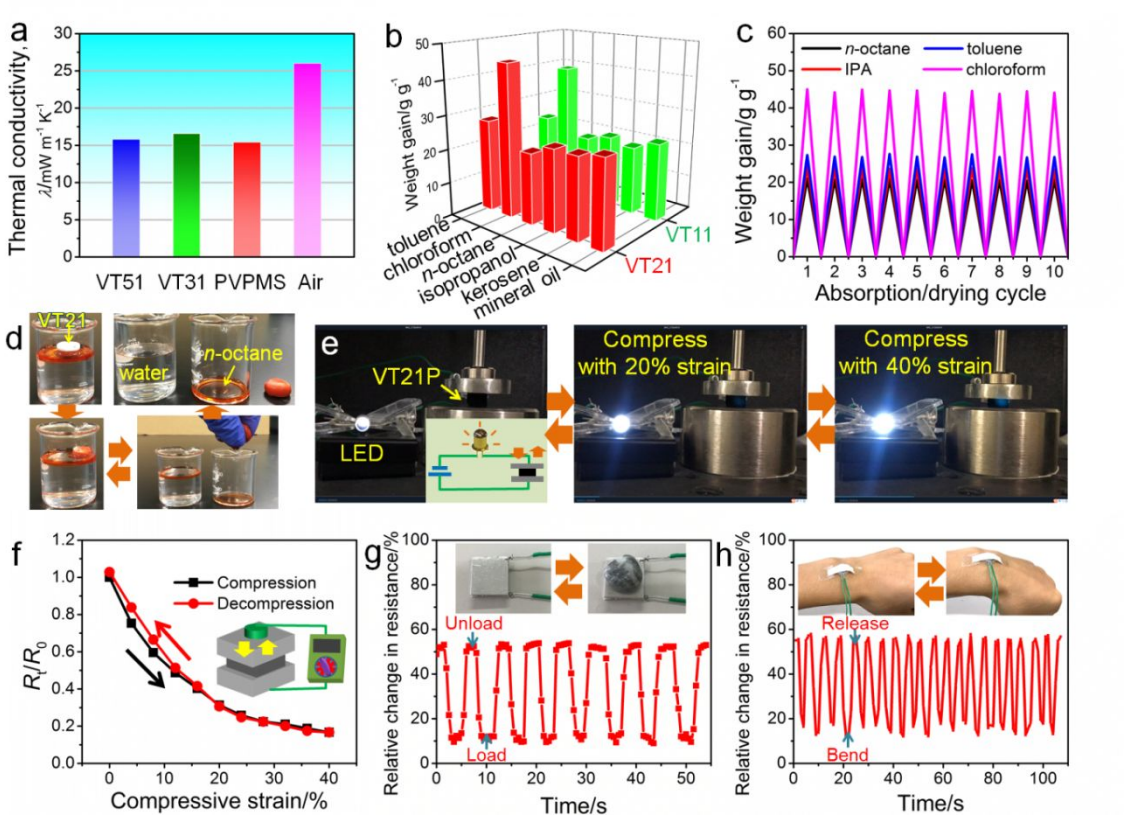

Fig. 6 (a) Thermal conductivities of typical aerogels. (b) Absorption capacities of typical aerogels for various organic solvents/oils. (c) Absorption/drying cycle performance of VT21 for *n*-octane, IPA, toluene, and chloroform. (d) Photographs of *n*-octane–water separation with VT21. (e) Strain-sensitive conductivity of VT21P. The inset is a schematic circuit. (f) Normalized electrical resistance versus compressive strain for VT21P. (g) Resistance response of VT21P as a pressure sensor upon loading and unloading a small stone for 8 cycles. (h) Resistance response of a sensor of VT21P upon bending and release of a wrist for 20 cycles.

Given their low bulk density (40–45 mg cm^{-3}) and highly porous structure with high hydrophobicity and high flexibility in both compression and bending, the copolymer aerogels VT21 and VT11 were supposed to possess excellent absorption of oils for oil–water separation. As shown in Fig. 6b, they exhibited high absorption capacity (2000–4500 %) for various organic solvents and oils such as toluene, chloroform, *n*-octane, 2-propanol (IPA), kerosene, and mineral oil. They also showed recyclability with an excellent absorption/drying cycle performance. They absorbed organic solvents such as *n*-octane, IPA, toluene, and chloroform quickly with their microstructure maintained, and absorption capacity was nearly unchanged after absorption and drying at 60 °C for 10 cycles (Fig. S8 and Fig. 6c). In addition, *n*-octane (colored with sudan III for visibility) was selectively absorbed quickly in monolithic VT21 in a two-phase system of *n*-octane and water and it was easily squeezed out, indicating excellent oil–water separation performance (Fig. 6d and Movie S3). The flexible copolymer aerogels were stable after squeezing for 10 times.

There were mainly two reasons why we choose VT21 and VT11 for absorption of organic solvents and oils. First, VT21 and VT11 exhibited much lower bulk density (40–45 mg cm^{-3}) compared to that of VT51 (210 mg cm^{-3}) and VT31(205 mg cm^{-3}). Therefore, the absorption capacity, defined as weight of absorbed liquid per 1 g of aerogel, of VT21 and VT11 for organic solvents and oils was supposed to be higher than those of VT51 and VT31. Second, VT21 and VT11 exhibited higher bending flexibility compared to that of VT51 and VT31. The higher bending flexibility enabled VT21 and VT11 to undergo repeated absorption/drying or absorption/squeezing without fracture, leading to better absorption/drying and absorption/squeezing cycle performances.

The absorption capacities for organic solvents or oils was higher than those of reported silica-polyHIPE aerogels and comparable to those of reported PVPDMS aerogels, polyimide, and sequential infiltration synthesis (SIS)/silane treated polyurethane.[38,45,46] Since the reported silica-polyHIPE aerogels were obtained *via* SD and PVPDMS aerogels were obtained *via* FD, the ambient-dried PVPMS/PVTMS copolymer aerogels showed advantages over them

for practical applications. The polyimide and (SIS)/silane treated polyurethane absorbed water except for organic solvents or oils, which showed lower absorption selectivity compared to that of the PVPMS/PVTMS copolymer aerogels.

Besides, the incorporation of PPy allowed the resulting flexible nanocomposite aerogel VT21P to be electrically conductive. A circuit connected with VT21P and a battery was able to light up a light-emitting diode (LED), and its brightness fluctuated upon compression and decompression of the aerogels, showing strain-sensitive conductivity (Fig. 6e and Movie S4). With increasing the compressive strain in the range of 0–40 %, the measured electrical resistance decreased significantly (83 % at 40 % strain) because of the more contacts among conductive PPy upon compression (Fig. 5), and recovered well upon decompression due to the spring-back phenomenon of the elastic aerogel (Fig. 6f). The response of resistance of VT21P upon loading and unloading a small stone has been demonstrated as a possible pressure sensor. The resistance changed with loading and unloading and exhibited good cycle performance (Fig. 6g). A pressure sensor of VT21P adhered to a wrist has also been demonstrated, in which the changes of resistance with bending and release of the wrist were clearly recorded (Fig. 6h). As discussed above, the compression cycle performance of VT21P was better than that of the reported PVPDMS/graphene composite aeroge. Therefore, the PVPMS/PVTMS/PPy nanocomposite aerogel was more suitable for strain sensing compared to PVPDMS/graphene composite aerogel. Comparison of typical properties of the copolymer aerogels and other reported similar aerogels was summarized in Table 3.

Table 3. Comparison of the copolymer aerogels and other reported similar aerogels: PMSQ aerogel,[44] PVSQ aerogel,[27] PVPMS aerogel,[36] and PVPDMS-based aerogel.[38]

Aerogel type	Sample	Drying method	ρ[a] /mg cm^3	WCA /°	D_m[b] /mm	Absorption capacity[c] /g/g	λ[d] /mW m^{-1} K^{-1}	Application
PMSQ aerogel	A10.0	APD	210	-	-	-	15.0	insulation
PVPSQ aerogel	VR-8	APD	170	-	-	-	15.3	insulation
PVPMS aerogel	AH1-48-1-100	APD	210	133	18	-	15.4	insulation
PVPDMS aerogel	PA1-2	FD	38	157	>30	28.4	-	absorption
PVPDMS/PVPMS aeogel	PA4	APD	190	142	29	-	16.2	insulation
	PA2-1	FD	54	157	>30	20.3	-	absorption
PVPDMS/graphene aerogel	PA2-G	FD	-	157	-	-	-	sensing
PVPMS/TMVS aerogel (this work)	VT51	APD	210	135	24	-	15.8	insulation
	VT21	APD	44	158	>35	27.3	-	absorption
PVPMS/TMVS/PPy aerogel (this work)	VT21P	APD	73	158	>35	-	-	sensing

[a] Bulk density. [b] Maximum diametral deflection of three-point bending tests with the fixture span of 25 mm on aerogels with thickness × width of 1 mm × 10 mm before fracture. [c] Absorption capacity for toluene. [d] Thermal conductivity at room temperature and ambient pressure.

Conclusions

In summary, new highly flexible aerogels based on a PVPMS/PVTMS co-network and its nanocomposite with PPy have been reported. The PVPMS/PVTMS copolymer aerogels have been synthesized by a facile approach involving consecutive radical co-polymerization and hydrolytic polycondensation from two precursors VMDMS and TMVS, followed by APD without any modification. The PVPMS/PVTMS/PPy nanocomposite aerogels have been prepared by an *in-situ* oxidation polymerization of pyrrole in the copolymer aerogels, followed by re-drying *via* APD. Highly porous elastic copolymer structures consisting of PMS and hydrocarbon polymers and the nanocomposite structures consisting of PMS, hydrocarbon polymers, and PPy have been obtained. The resulting aerogels exhibit tunable crosslinking density, tunable bulk density (40–210 mg cm^{-3}) and sizes of pores (10 nm–15 μm) and particulate skeletons (20 nm–3 μm), good hydrophobicity, and high flexibility in both compression and bending. More importantly, these aerogels combine excellent thermal insulation (λ=15.8–16.6 mW m^{-1} K^{-1}), oil-water separation, and pressure sensing. This work will open a new way to flexible design of soft porous functional materials towards practical applications in thermal insulation, separation, and pressure sensing.

Materials and methods

Materials

Vinylmethyldimethoxysilane (VMDMS), tetramethylammonium hydroxide (TMAOH, 25 wt % in water), and iron (III) chloride hexahydrate ($FeCl_3 \cdot 6H_2O$) were purchased from Sigma-Aldrich, Co. (USA). Distilled water was obtained from Hayashi Pure Chemical Ind., Ltd. (Japan). Trimethylvinylsilane (TMVS), di-*tert*-butyl peroxide (DTBP), and pyrrole were obtained from Tokyo Chemical Industry Co., Ltd. (Japan). Benzyl alcohol (BzOH), 2-propanol (IPA), methanol (MeOH), and *n*-hexane were purchased from Kishida Chemical Co., Ltd. (Japan). All the chemicals were used as received.

Sample Preparation

A given amount of the precursors VMDMS and TMVS with the molar ratio of 5:1, 3:1, 2:1, or 1:1 and initiator DTBP (1 mol %) were mixed and charged in a hydrothermal reactor. The reactor was sealed after being flushed with Ar and then heated at 120 °C for 48 h to promote radical co-polymerization of the precursors. After cooling naturally at room temperature, a transparent and viscous liquid that mainly contains polyvinylmethyldimethoxysilane

(PVMDMS)/polyvinyltrimethylsilane (PVTMS) copolymer was obtained. BzOH, H_2O, and TMAOH with a given molar ratio were added to the above liquid in the listed order under stirring. The detailed starting compositions were shown in Table 2. After stirring for 5 min, the mixture was then transferred into a container, which was then sealed and placed in a forced convection oven at 100 °C, where the gel formed within 1 h and was aged for 4−5 d. The gels of VT51 and VT31 were aged for 4 d, while the gels of VT21 and VT11 were aged for 5 d. After solvent exchange with IPA and *n*-hexane, the gel was dried by evaporation at ambient pressure and room temperature for 2−4 d and at 80 °C for 4 h to obtain a copolymer aerogel.

An appropriate amount of $FeCl_3{\cdot}6H_2O$, H_2O, and MeOH were mixed at 4 °C. Pyrrole was then added to the mixture under stirring at 4 °C. The molar ratio of pyrrole:$FeCl_3{\cdot}6H_2O$: H_2O: MeOH was fixed at 1:2:77:51. After stirring for 10 s, a typical copolymer aerogel was immersed in the above mixture that contains pyrrole. The mixture was absorbed in aerogel quickly, allowing pyrrole to be polymerized in the aerogel network, forming polypyrrole (PPy) in aerogel. The PVPMS/PVTMS/PPy composite gel was obtained after reaction at room temperature for 24 h. The composite gel was taken out and subjected to solvent exchange with IPA and *n*-hexane. Finally, the gel was dried by evaporation at ambient pressure and 80 °C for 4 h to afford a PVPMS/PVTMS/PPy aerogel.

Characterizations

The chemical structure of aerogels was investigated by a Fourier transform infrared (FTIR) spectroscope (IRAffinity-1, Shimadzu Corp., Japan). The chemical structure was also studied by the ^{29}Si cross-polarization magic angle spinning (CP/MAS) nuclear magnetic resonance (NMR) spectroscopy with an 800 MHz NMR spectrometer (Avance III 800US Plus, Bruker Corp., Germany) under the static magnetic field of 18.8 T. It was operated with a double resonance probe with 4 mm MAS probe head and with hexamethylcyclotrisiloxane as an external reference material. The MAS frequency was kept at 12 kHz, the number of scans was 4096, contact time for CP process was 5.5 ms, and the recycle delay was 3 s. The weight-average molecular weight (M_w) and polydispersity (M_w/M_n) of PVMDMS/PVTMS copolymer were measured using a gel permeation chromatography (GPC) system (GPC104, Shodex, Japan) with an LF604 column and a chloroform solvent. The resulting polymers after radical polymerization was completely dissolved in chloroform solvent for the GPC measurement.

The morphology was observed with a field emission scanning electron microscope (FESEM, JSM-6700F, JEOL, Japan) and a scanning electron microscope (SEM, JSM-6060S, JEOL, Japan). The N_2 adsorption−desorption isotherm, specific surface area, and pore size distribution were determined by a N_2 adsorption analyzer (BELSORP-mini, BEL Japan, Inc., Japan). The specific surface area was derived from the adsorption branch by the Brunauer−Emmett−Teller (BET) method, while the pore size distribution was obtained from the adsorption branch using the Barrett−Joyner−Halenda (BJH) calculation.

Bulk density was obtained by measuring the mass, height, and diameter of cylindrical aerogels. The visible-light transmittance of aerogels was determined by a UV−Vis−NIR spectrophotometer (V-670, JASCO, Japan) equipped with an integrating sphere. Water contact angles on aerogels were measured by Drop Master (DM-561Hi, Kyowa Interface Science Co., Ltd., Japan) with the water droplet volume of 3 μL.

Stress−strain curves of uniaxial compression−decompression tests and three-point bending tests were measured with a material tester (EZGraph, Shimadzu Corp., Japan). The cross-head speed for compression and bending tests was 10 and 2 mm min^{-1}, respectively. For the uniaxial compression-decompression tests, cylindrical specimens with a height of 4−15 mm and a diameter of 8−18 mm were used. For the three-point bending tests, sheet-shaped specimens with width × length × thickness of 10 × (60−70) × 1 mm were used. The fixture span in three-point bending tests was set to 25 mm.

The thermal conductivity of aerogels was measured with a heat flow meter (HFM 436 Lambda, NETZSCH, Germany) at room temperature and ambient pressure. Aerogel plates with width × length × thickness of 100 × 100 × 10 mm were used.

The absorption performance of aerogels was investigated by immersing aerogels into different solvents or oils and measuring the weight of the samples before and after absorption. Absorption capacity was determined by equation $W = (M-M_0)/M_0$, where M_0 is weight before absorption, M is weight after saturated absorption, and W is weight gain. Absorption/drying cycle performance was investigated by immersing aerogels in various solvents and drying at 80 °C for 10 cycles.

Electrical resistance−compressive strain curves of aerogels were measured using a material tester mentioned above and an ohmmeter (M-04, Custom Corp., Japan) *via* a two-probe method. A cylindrical or cubic aerogel was loaded between two metallic compression plates of the material tester. The two compression plates were attached by copper wires to the ohmmeter for the electrical resistance measurement during compression and decompression of aerogels.

Conflicts of interest

There are no conflicts to declare.

Acknowledgements

This work was financially supported by the Advanced Low Carbon Technology Research and Development Program (ALCA, JST Japan), Japan Society for the Promotion of Science (JSPS) KAKENHI (17K06015), Incubation Program of Kyoto University, and National Key Research and Development Program of China (2017YFA0204600). Prof. Shigeru Yamago and Dr. Takehiro Fujita at Institute for Chemical Research, Kyoto University, are acknowledged for their help in GPC. The CP/MAS NMR measurements were carried out in the JURC at the same institute.

Notes and references

1 J. Fricke, *Nature*, 1995, **374**, 409−410.
2 N. Husing and U. Schubert, *Angew. Chem. Int. Ed.*, 1998, **37**, 22−45.

3 S. O. Kucheyev, M. Stadermann, S. J. Shin, J. H. Satcher Jr., S. A. Gammon, S. A. Letts, T. van Buuren and A. V. Hamza, *Adv. Mater.*, 2012, **24**, 776–780.
4 Z. Wang, Z. Dai, J. Wu, N. Zhao and J. Xu, *Adv. Mater.*, 2013, **25**, 4494–4497.
5 C. -B. Ma, B. Du and E. Wang, *Adv. Funct. Mater.*, 2017, **27**, 1604423–1604431.
6 X. Lu, M. C. Arduini-Schuster, J. Kuhn, O. Nilsson, J. Fricke and R. W. Pekala, *Science*, 1992, **255**, 971–972.
7 J. Fan, S. Hui, T. P. Bailey, A. Page, C. Uher and F. Yuan, *J. Mater. Chem. A* **2019**, 7, 1574–1584.
8 Y. Kobayashi, T. Saito and A. Isogai, *Angew. Chem., Int. Ed.*, 2014, **53**, 10394–10397.
9 Y. Fan, W. Ma, D. Han, S. Gan, X. Dong and L. Niu, *Adv. Mater.*, 2015, **27**, 3767–3773.
10 H. Maleki and N. Husing, *Appl. Catal. B: Environ.*, 2018, **221**, 530–555.
11 G. Zu, J. shen, L. Zou, F. Wang, X. Wang, Y. Zhang and X. Yao, *Carbon*, 2016, **99**, 203–211.
12 M. Antonietti, N. Fechler and T. -P. Fellinger, *Chem. Mater.*, 2014, **26**, 196–210.
13 Y. Si, X. Wang, C. Yan, L. Yang, J. Yu and B. Ding, *Adv. Mater.*, 2016, **28**, 9512–9518.
14 A. C. Pierre and G. M. Pajonk, *Chem. Rev.*, 2002, **102**, 4243–4265.
15 N. Leventis, *Acc. Chem. Res.*, 2007, **40**, 874–884.
16 D. P. Mohite, Z. J. Larimore, H. Lu, J. T. Mang, C. Sotiriou-Leventis and N. Leventis, *Chem. Mater.*, 2012, **24**, 3434–3448.
17 J. P. Randall, M. A. B. Meador and S. C. Jana, *ACS Appl. Mater. Interfaces*, 2011, **3**, 613–626.
18 X. Wang and S. C. Jana, *ACS Appl. Mater. Interfaces*, 2013, **5**, 6423–6429.
19 M. A. B. Meador, E. J. Malow, R. Silva, S. Wright, D. Quade, S. L. Vivod, H. Guo, J. Guo and M. Cakmak, *ACS Appl. Mater. Interfaces*, 2012, **4**, 536–544.
20 G. Hasegawa, T. Shimizu, K. Kanamori, A. Maeno, H. Kaji and K. Nakanishi, *Chem. Mater.*, 2017, **29**, 2122–2134.
21 Z. U. Khan, J. Edberg, M. M. Hamedi, R. Gabrielsson, H. Granberg, L. Wagberg and I. Engquist, *Adv. Mater.*, 2016, **28**, 4556–4562.
22 S. Takeshita and S. Yoda, *Chem. Mater.*, 2015, **27**, 7569–7572.
23 J. Song, C. Chen, Z. Yang, Y. Kuang, T. Li, Y. Li, H. Huang, I. Kierzewski, B. Liu, S. He, T. Gao, S. U. Yuruker, A. Gong, B. Yang and L. Hu, *ACS Nano*, 2018, **12**, 140–147.
24 Y. Si, J. Yu, X. Tang, J. Ge and B. Ding, *Nat. Commun.*, 2014, **5**, 5802–5810.
25 M. Yang, N. Zhao, Y. Cui, W. Gao, Q. Zhao, C. Gao, H. Bai and T. Xie, *ACS Nano*, 2017, **11**, 6817–6824.
26 F. Guo, Y. Jiang, Z. Xu, Y. Xiao, B. Fang, Y. Liu, W. Gao, P. Zhao, H. Wang and C. Gao, *Nat. Commun.*, 2018, **9**, 881–889.
27 T. Shimizu, K. Kanamori, A. Maeno, H. Kaji, C. M. Doherty, P. Falcaro and K. Nakanishi, *Chem. Mater.*, 2016, **28**, 6860–6868.
28 K. Kanamori, M. Aizawa, K. Nakanishi and T. Hanada, *Adv. Mater.*, 2007, **19**, 1589–1593.
29 S. Yun, H. Luo and Y. Gao, *J. Mater. Chem. A*, 2015, **3**, 3390–3398.
30 Y. Ma, Y. Yue, H. Zhang, F. Cheng, W. Zhao, J. Rao, S. Luo, J. Wang, X. Jiang, Z. Liu, N. Liu and Y. Gao, *ACS Nano*, 2018, **12**, 3209–3216.
31 B. Qiu, M. Xing and J. Zhang, *J. Am. Chem. Soc.*, 2014, **136**, 5852–5855.
32 S. S. Prakash, C. J. Brinker, A. J. Hurd and S. M. Rao, *Nature*, 1995, **374**, 439–443.
33 L. Su, H. Wang, M. Niu, X. Fan, M. Ma, Z. Shi and S. -W. Guo, *ACS Nano*, 2018, **12**, 3103–3111.
34 A. S. Dorcheh and M. H. Abbasi, *J. Mater. Process. Technol.*, 2008, **199**, 10–26.
35 L. Huber, S. Zhao, W. J. Malfait, S. Vares and M. M. Koebel, *Angew. Chem., Int. Ed.*, 2017, **56**, 4753–4756.
36 G. Zu, T. Shimizu, K. Kanamori, Y. Zhu, A. Maeno, H. Kaji, J. Shen and K. Nakanishi, *ACS Nano*, 2018, **12**, 521–532.
37 G. Zu, K. Kanamori, T. Shimizu, Y. Zhu, A. Maeno, H. Kaji, K. Nakanishi and J. Shen, *Chem. Mater.*, 2018, **30**, 2759–2770.
38 G. Zu, K. Kanamori, A. Maeno, H. Kaji and K. Nakanishi, *Angew. Chem. Int. Ed.*, 2018, **57**, 9722–9727.
39 D. J. T. Hill, C. M. L. Preston and A. K. Whittaker, *Polymer*, 2002, **43**, 1051–1059.
40 T. Matias, C. Varino, H. C. de Sousa, M. E. M. Braga, A. Portugal, J. F. J. Coelho and L. Duraes, *J. Mater. Sci.*, 2016, **51**, 6781–6792.
41 A. Salabat, F. Mirhoseini, M. Arjomandzadegan and E. A. Jiryaei, *New J. Chem.*, 2017, **41**, 12892–12900.
42 J. -X. Feng, H. Xu, S. -H. Ye, G. Ouyang, Y. -X. Tong and G. -R. Li, *Angew. Chem. Int. Ed.*, 2017, **56**, 8120–8124.
43 J. C. H. Wong, H. Kaymak, S. Brunner and M. M. Koebel, *Microporous Mesoporous Mater.*, 2014, **183**, 23–29.
44 G. Hayase, K. Kugimiya, M. Ogawa, Y. Kodera, K. Kanamori and K. Nakanishi, *J. Mater. Chem. A*, 2014, **2**, 6525–6531.
45 D. B. Mahadik, K. -Y. Lee, R. V. Ghorpade and H. -H. Park, *Sci. Rep.*, 2018, **8**, 16783–16791.
46 E. Barry, A. U. Mane, J. A. Libera, J. W. Elam and S. B. Darling, *J. Mater. Chem. A*, 2017, **5**, 2929–2935.

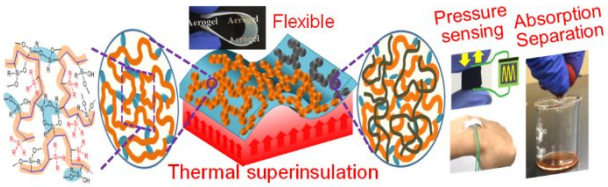

TOC Graphic

Highly flexible copolymer and copolymer/polypyrrole nanocomposite aerogels have been synthesized via ambient pressure drying for superinsulation, separation and pressure sensing.